

The Polarimetric Capabilities of NICMOS

D. C. Hines¹, G. D. Schmidt & Dyer Lytle¹

Steward Observatory, The University of Arizona, Tucson, AZ 85721

Abstract. The polarimetric capabilities of NICMOS are demonstrated from data obtained during the Early Release Observations of IRC +10216 and CRL 2688 (the Egg Nebula). Preflight Thermal Vacuum tests revealed that each polarizer has a unique polarizing efficiency, and that the position angle offsets differ from the nominal positions of 0°, 120° & 240°. Therefore an algorithm different from that of an ideal polarizer is required for proper reduction of astronomical polarimetry data. We discuss this new algorithm and the results of its application to NICMOS data.

We also present preliminary estimates of the Instrumental Polarization, the sensitivity of the grisms to polarized light, and the accuracy of NICMOS imaging polarimetry for faint and low polarization objects. Finally, we suggest strategies for maximizing the success of NICMOS polarimetry observations.

1. Introduction

Studies of polarized light have effected profound changes in our understanding of astronomical objects, especially within the last two decades with the advent of sensitive, large format imaging arrays such as optical CCDs and the NICMOS3 infrared detectors. Imaging of linearly polarized light from young stellar objects, bipolar nebulae, radio galaxies and hyperluminous infrared galaxies has shown that disks of dusty gas play a key role in the birth and death of stars, and can strongly influence the appearance of quasars and QSOs.

The Near Infrared Camera and Multi-Object Spectrometer (NICMOS) contains optical elements which enable high spatial resolution, high sensitivity observations of linearly polarized light from 0.8–2.1 μm . The filter wheels for Camera 1 (NIC1) and Camera 2 (NIC2) each contain three polarizing elements sandwiched with a band-pass filter. The design specifies that the position angle of the primary axis of each polarizer projected onto the detector be offset by 120° from its neighbor, and that the polarizers have identical efficiencies. While this clean concept was not strictly achieved, the reduction techniques described below permit accurate polarimetry to be carried out with both the short- and long-wavelength cameras over their full fields of view.

2. Thermal Vacuum Tests

The preflight thermal vacuum test program for NICMOS included an extensive characterization of the polarimetry optics and the overall sensitivity of the non-polarimetry optics to polarized light. Uniform illumination of the entire camera field with light of known polarization and position angle was provided by a calibration polarizer attached to the CIRCE standard light source.

¹NICMOS Project, The University of Arizona

Images were obtained as a function of the calibration polarizer position angle with and without the NICMOS polarizers in place to determine the polarizing efficiencies,¹ the absolute position angles of the NICMOS polarizers with respect to the NICMOS entrance aperture, and to evaluate the polarization signature imparted by the mirrors which comprise the NICMOS imaging system. Images were also obtained with the grisms of Camera 3 to characterize their sensitivity to polarized light.

The Thermal Vacuum tests showed that:

- Each polarizer has a unique polarizing efficiency, with the POL120S having a very low efficiency of only 48%.
- The offsets between the position angles of the polarizers within each filter wheel differ from their nominal values of 120°.
- The polarization induced by the mirrors in the NICMOS optical train appears to be small ($\lesssim 1\%$).
- The grisms are slightly sensitive to the orientation of incoming polarized light, with G206 showing the largest variation in intensity ($\sim 5\%$) for completely polarized light. This effect scales with percentage polarization and will be negligible for the majority of astronomical situations.

3. The HSL Algorithm for Reducing NICMOS Polarimetry Observations

The “standard theory” algorithm for polarimetry data reduction as outlined in the original NICMOS Manual (Axon et al., 1996) assumes that the polarizers have uniform and perfect (100%) polarizing efficiencies, and that the projected position angles of the primary axis of the polarizers are offset by exactly 120°. The thermal vacuum tests showed that the NICMOS polarizers are not ideal, so a more complex technique is required. The new algorithm developed by Hines, Schmidt & Lytle (hereafter HSL) is presented below.

The observed signal from a polarized source of total intensity I and linear Stokes parameters Q and U measured through the k^{th} polarizer oriented with a position angle² ϕ_k is

$$S_k = A_k I + \epsilon_k (B_k Q + C_k U), \quad (1)$$

where

$$A_k = \frac{1}{2} t_k (1 + l_k), \quad B_k = A_k \cos 2\phi_k, \quad C_k = A_k \sin 2\phi_k,$$

and ϵ_k is the polarizing efficiency, t_k is the fraction of light transmitted for a 100% polarized input aligned with the polarizer’s axis, and l_k is the fraction transmitted (exclusive of that involved in t_k) when the incoming light is perpendicular to the axis of the polarizer (see Table 1). After solving this system of equations to derive the Stokes parameters at each pixel (I, Q, U), the percentage polarization (p) and position angle (θ) at that pixel are calculated in the standard way:

$$p = 100\% \times \frac{\sqrt{Q^2 + U^2}}{I}, \quad \text{PA} = \frac{1}{2} \tan^{-1} \left(\frac{U}{Q} \right).$$

¹Polarizer efficiency is defined as $\epsilon = (S_{\text{par}} - S_{\text{perp}})/(S_{\text{par}} + S_{\text{perp}})$, where S_{par} and S_{perp} are the respective measured signals for a polarizer oriented parallel and perpendicular to the axis of a fully polarized beam.

²Polarizer position angle as measured from the NICMOS Aperture Offset Angle of 224.52°, about the aperture center toward the +U3 axis.

[Note that the arc-tangent function is implemented differently on different systems and programming environments, so care must be taken to ensure that the derived angles place the electric vector in the correct quadrant.]

Table 1 presents the properties of the individual polarizers, and Table 2 lists the coefficients derived from these parameters for use in solving Equation 1.

Table 1. Characteristics of Polarizers:

Filter	ϕ_k^a	ϵ_k	t_k	l_k	Comments
POL0S	1.42	0.9717	0.7760	0.0144	...
POL120S	116.30	0.4771	0.7760	0.3540	Possible “ghost” images
POL240S	258.72	0.7682	0.7760	0.1311	...
POL0L	8.84	0.7313	0.9667	0.1552	...
POL120L	131.42	0.6288	0.9667	0.2279	...
POL240L	248.18	0.8738	0.9667	0.0673	...

^aAs measured from the NICMOS aperture 224.52° about the +U3 axis.

Table 2. Coefficients for Simultaneous Solution of Equation 1:

Filter	A_k	$\epsilon_k * B_k$	$\epsilon_k * C_k$
POL0S	+0.3936	+0.3820	+0.0189
POL120S	+0.5253	-0.1522	-0.1991
POL240S	+0.4389	-0.3113	+0.1293
POL0L	+0.5584	+0.3890	+0.1240
POL120L	+0.5935	-0.0465	-0.3703
POL240L	+0.5159	-0.3262	+0.3111

4. On-Orbit Results

Polarimetry data were obtained for IRC +10216 and CRL 2688 in NIC1 and NIC2 respectively as part of the Early Release Observations program. The descriptions of the observations can be obtained on the STScI website via the Cycle 7 proposal number or PI name (ERO 7120: Skinner; ERO 7115: Hines). Overall, the NICMOS and ground-based polarimetry agree remarkably well, once the NICMOS polarimetric images are binned to match the spatial resolution of the ground-based images.

4.1. NIC1 — IRC +10216

Figure 1 presents the NICMOS polarimetry results for IRC +10216 (Skinner et al. 1997) compared with the available ground-based data from Kastner & Weintraub (1994). The polarization map derived by processing the NICMOS data with the new HSL algorithm (center panel) agree well with the ground based data. In contrast, polarization images derived by using the “standard theory” underestimate the polarization and lead to incorrectly oriented electric vector position angles.

Variations of the percentage polarization in relatively uniform regions of the HSL-reduced IRC +10216 data suggest uncertainties $\sigma_{p,\text{meas}} \sim 3\text{--}5\%$ (in percentage polarization per pixel), and comparison with the ground-based data suggests an uncertainty in the position angles $\sim 2^\circ$ in a 5×5 pixel bins (Figure 1).

J-Band Imaging Polarimetry of IRC +10216

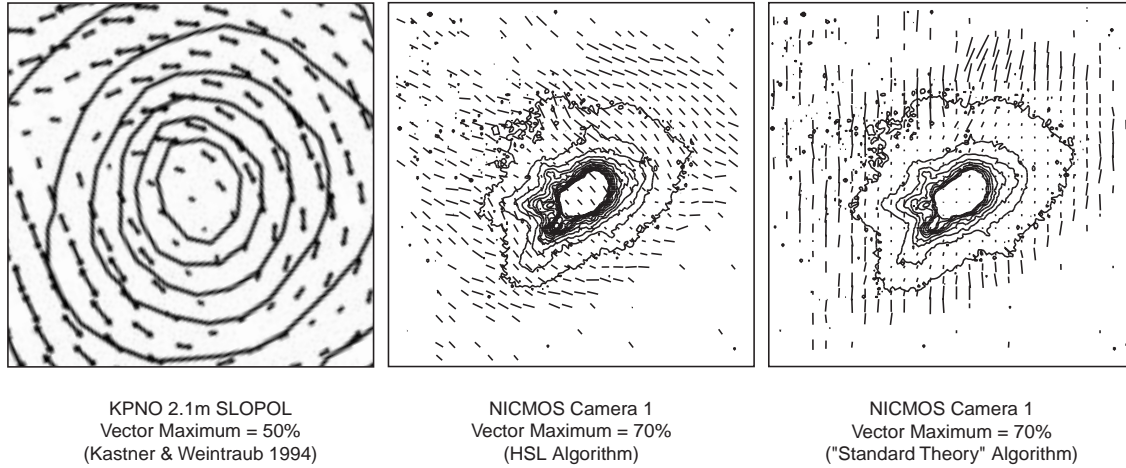


Figure 1. J-Band Imaging Polarimetry of IRC +10216 observed from the ground (Kastner & Weintraub 1994), compared with data obtained using NICMOS Camera 1 and reduced with the HSL and “standard theory” algorithms. The data reduced with the HSL algorithm agree well with the ground based data. For clarity, the NICMOS polarization vectors are plotted for 5×5 pixel bins, and the faintest and brightest intensity contours have been omitted.

4.2. NIC2 — CRL 2688

Figure 2 presents the NICMOS polarimetry results for CRL 2688 compared with observations obtained from the ground (Sahai et al. 1997). In this case the ground-based data are of exceptional quality and allow a more detailed comparison than for IRC +10216. Overall, the NICMOS and ground-based data agree quite well and show centrosymmetric patterns of position angle within the polar lobes.

Other, more subtle, features of the polarization morphology that are seen in the ground-based polarization map are reproduced precisely in the NICMOS map, confirming that the NICMOS polarimetry is well calibrated. However, the superior resolution of the NICMOS data reveals polarization features that are not apparent in the ground-based polarization map. In particular we note the very high polarizations (~ 70 – 85%) in the arcs and filamentary structure — features that are washed out (beam averaged) in the ground-based images resulting in lower observed polarization.

As for IRC +10216, uncertainties in the spacecraft data are estimated to be ~ 3 – 5% in percentage polarization, and $\sim 2^\circ$ in the position angles.

5. Recommended Strategies

As illustrated by the EROs discussed above, the NICMOS system is capable of producing accurate polarimetry for highly polarized objects.

Limiting Polarization: Because the errors for percentage polarization follow a Rice distribution, precise polarimetry requires measurements such that $p/\sigma_{p,\text{meas}} > 4$ (Simmons & Stewart 1985). Therefore, the preliminary uncertainty estimates discussed above $\sigma_{p,\text{meas}} \approx 3$ – 5% (per pixel) imply that objects should have polarizations of at least 12–20%

CRL 2688 — The Egg Nebula

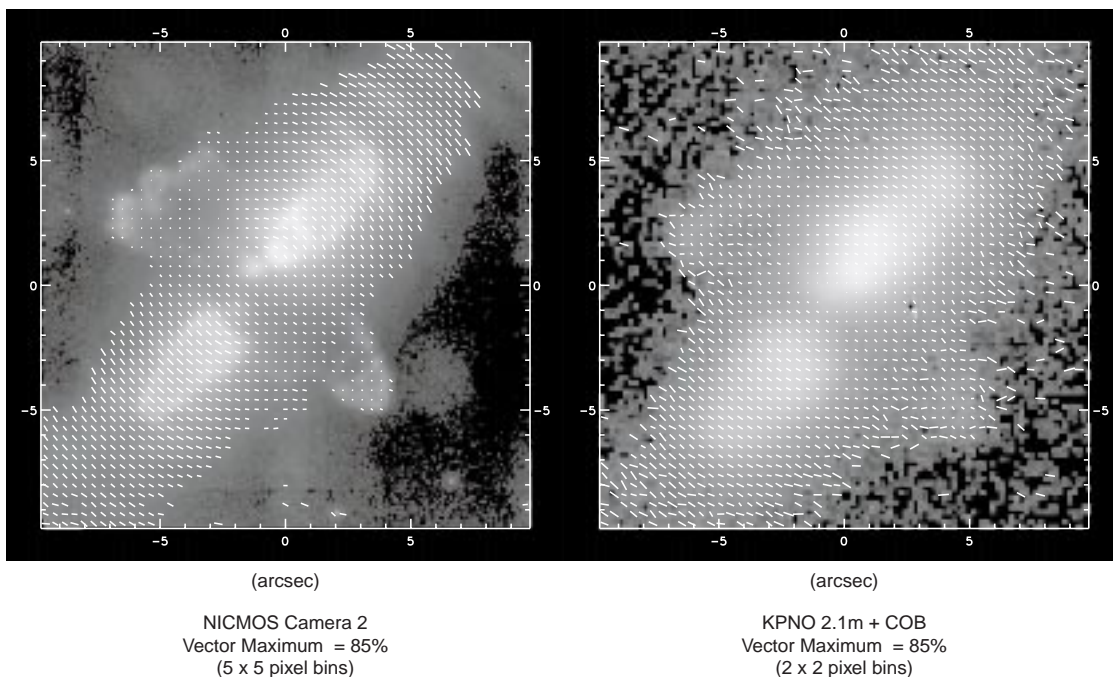


Figure 2. K-band Imaging Polarimetry of CRL 2688 (The Egg Nebula) using NICMOS Camera 2, and the Cryogenic Optical Bench (COB) attached to the 2.1m at Kitt Peak. For clarity, the vectors in the NICMOS and COB data are binned by 5×5 and 4×4 pixels respectively.

per pixel. Our experiments show that binning the Stokes parameters before forming the percentage polarization (p) and the position angles reduces the uncertainties by $\sim 1/\sqrt{N}$, where N is the number of pixels in the bin (see Limiting Brightness discussion below). In principle, uncertainties as low as 1% should be achievable with bright objects.

In addition, the instrumental polarization (IP) is still unknown. The thermal vacuum tests suggest that it will be about 1%, but preliminary results from the Cycle 7 calibration program indicate that this may be an underestimate. Until *both* the magnitude and position angle of the IP are well established, the IP should be treated as an unknown quantity.

Limiting Brightness of the Target: In a perfect photon-counting system, $\sigma_{p,\text{phot}} \approx \sqrt{2/E}$, where E is the total number of photons counted. For CRL 2688, the signal strength even in regions of low intensity (e.g. the H_2 -emitting torus) should have produced $\sigma_{p,\text{phot}} \approx 1\%$, but we measure $\sigma_{p,\text{meas}} \approx 3\text{--}5\%$, which suggests that the uncertainties are dominated by noise other than that from the source itself. Conservatively, integration times should be set such that the $\sigma_{p,\text{phot}} < 4\sigma_{p,\text{meas}}$.

Position Angle of Incoming Polarization Relative to NICMOS Orientation: Because of the non-optimum polarizer orientations and efficiencies, the uncertainty in polarization is also a function of the position angle of the electric vector of the incoming light. For observations with low signal-to-noise ratios (per polarizer image), and targets with lower polarizations, the difference between the signals in the images from the three polarizers becomes dominated by photon noise rather than analyzed polarization signal. Therefore, observations that place important incoming electric vectors at $\approx 45^\circ$ and $\approx 135^\circ$

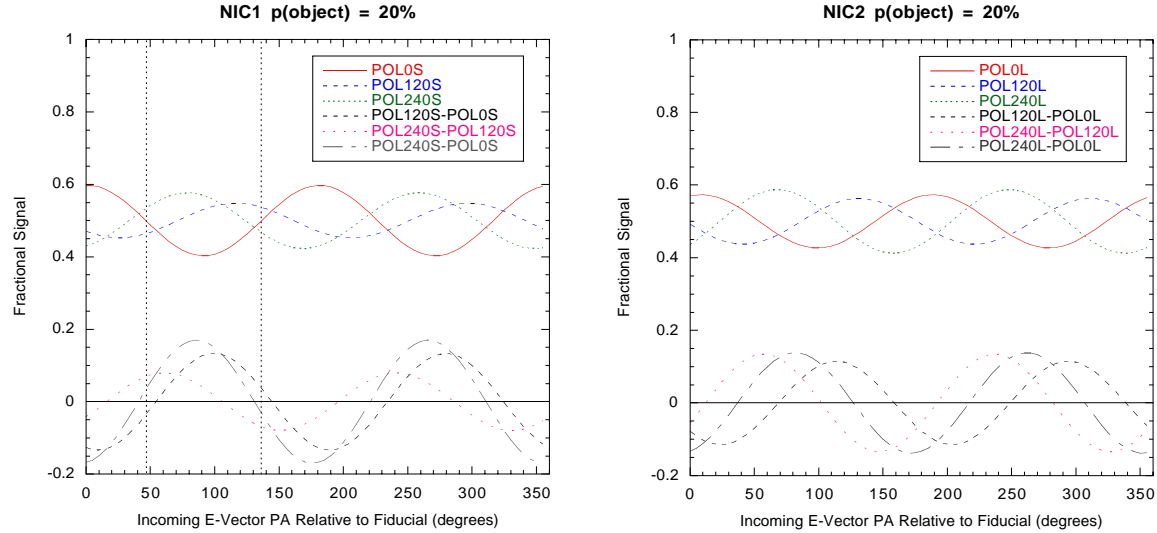


Figure 3. Fractional signal measured in each NICMOS polarizer as a function of incident electric vector position angle (PA) for 20% polarized light. The lower curves are the differences in fractional signal between images taken with successive polarizers. The vertical dashed lines in the left panel (NIC1) represent the position angles where these differences are all small.

in the NICMOS aperture reference frame should be avoided in NIC1. No such restriction is necessary for NIC2.

6. Future Directions

The Cycle 7 calibration program will observe several polarized and unpolarized targets in both cameras to measure the instrumental polarization and verify the absolute position angle calibration. These observations will be repeated later in the season when the spacecraft is oriented 90° with respect to the initial observations, thus allowing a unique determination of the instrumental polarization. In addition, the redundant data sets will allow a more detailed characterization of the polarization uncertainties.

Acknowledgments. It is a pleasure to thank B. Stobie, L. Bergeron and A. Evans for assistance with the (non-polarimetric) data calibration. We also thank Joel Kastner for the use of his COB observations of CRL 2688 in advance of publication, and Chris Skinner for making the IRC +10216 data available. DCH acknowledges support from the NICMOS project under NASA grant NAG 5-3042.

References

- Axon, D., et al., 1996, *NICMOS Instrument Handbook*, Version 1.0 (Baltimore: STScI).
 Kastner, J. & Weintraub, D. 1994, *ApJ*, 434, 719.
 Sahai, R., Hines, D. C., Kastner, J. H., Weintraub, D. A., Trauger, J. T., Rieke, M. J., Thompson, R. I. & Schneider, G., 1997, *ApJ*, in press.
 Skinner, C.J., et al., 1997, in prep.
 Simmons, J.F.L. & Stewart, B.G, 1985, *A&A*, 142, 100.